Photoionization of atomic barium including effects of relaxation and polarization

Mickey Kutzner, Zikri Altun,* and Hugh P. Kelly
Jesse W. Beams Laboratory of Physics, Department of Physics, University of Virginia, Charlottesville, Virginia 22901
(Received 1 June 1989)

The photoionization cross sections of the $4d^{10}$, $5s^2$, $5p^6$, and $6s^2$ subshells of atomic barium and the angular distribution asymmetry parameters for the $4d^{10}$ and $5p^6$ subshells have been calculated using many-body perturbation theory. Our main purpose is to determine whether relaxation and polarization effects can account for the large difference between recent 4*d* photoemission experiments and total absorption experiments. Coupling between a number of *LS*-coupled final-state channels has been included. Relaxation effects have been included by evaluating many-body diagrams and also by calculating excited orbitals in the field of the relaxed ionic core. In the latter case, overlap integrals between initial- and final-state orbitals of the spectator electrons were included. Polarization effects have been included by evaluating many-body diagrams. Results are compared with experiments and other calculations.

I. INTRODUCTION

The inner-shell 4*d* photoionization spectra of atomic lanthanides and the preceding elements (i.e., Xe, Cs, Ba) are characterized by broad, delayed absorption peaks. These strong absorption resonances are often called giant resonances and have been the topic of much recent discussion.[1] Few cases of giant resonances have been studied as carefully by experimentalists and theorists as the shape resonance observed in barium ($Z=56$) above the 4*d* ionization threshold.

The first data available for barium were relative measurements of the total absorption cross section.[2–7] These total absorption measurements are reproduced quite well by recent calculations, e.g., the random-phase approximation with exchange modified to include relaxation effects[8,9] (RPAER), low-order many-body perturbation theory[10,11] (MBPT), and the time-dependent local-density approximation[12,13] (TDLDA). The inclusion of relaxation effects is an essential ingredient for all calculations (other than the TDLDA) that successfully reproduce the total absorption results. The first two methods account for relaxation of the core by calculating excited-state wave functions in the field of the self-consistent ionic core. Calculations such as the RPAE which do not include relaxation yield a peak in the cross section that is too narrow and too close to the 4*d* threshold.[9,10]

Recently, photoelectron spectroscopy has been used to partition the total cross section into partial cross sections. Photoemission results on solid-phase Ba were obtained by Hecht and Lindau,[5] who found that the large contribution of the 4*d* and the small contributions of the 5*p* and 5*s* partial cross sections accounted for almost all of the absorption. Satellite structure was found to be a small fraction of the total emission, and direct two-electron continuum emission was assumed to be negligible. More recently, Becker and co-workers[14,15] have partitioned the vapor phase measurements of Richter *et al.*[7] and found that a significant fraction of the absorption is due to satellites. In some regions the satellite emission nearly equals the 4*d* emission. The 4*d* partial cross section is found by Becker *et al.*[14] to obtain a peak value of only 21.7 Mb compared with a peak in the total absorption of 38.8 Mb.[7] Bizau *et al.*[16] have measured the relative strengths of the 4*d*, 5*p*, 5*s*, and 6*s* cross sections in the region of the giant 4*d* resonance and have found that, upon normalizing the 5*p* measurement to the TDLDA calculation,[13] the 4*d* partial cross section is even lower than that of Becker *et al.*[14] at the absorption maximum. It has recently been found[17] that inclusion of interchannel coupling and relaxation effects, as well as overlap integrals between the ground-state orbitals and relaxed final-state orbitals, yields fairly good agreement between theory and the experiments.[14,16]

In this paper we investigate whether the inclusion of higher-order many-body diagrams in the theoretical calculations can account for the results of Becker *et al.*[14] and Bizau *et al.*[16] from a perturbation-theory approach without resorting to the relaxed-orbital model. We have examined core relaxation, polarization, and other higher-order effects on the 4*d* partial cross section and we compare the results with the experimental photoemission data. The influence of relaxation effects on the 5*p* cross section is also evaluated using the relaxed-orbital model near the 5*p* threshold. In Sec. II, we briefly review aspects of the many-body perturbation theory that are pertinent to this problem. Section III contains computational details of calculations. The results of our present calculations are compared with experiment and with previous calculations in Sec. IV. In Sec. V we discuss our results and present conclusions.

II. THEORY AND METHODS

A. The perturbation expansion

The photoionization cross section in the electric dipole approximation is given by[18]

$$\sigma(\omega)=\frac{4\pi\omega}{c}\mathrm{Im}\alpha(\omega)\ , \tag{1}$$

where $\mathrm{Im}\alpha(\omega)$ represents the imaginary part of the frequency-dependent dipole polarizability for the atom. Atomic units are used throughout the paper.

We apply MBPT to calculate $\mathrm{Im}\alpha(\omega)$, which can be expressed in terms of many-particle dipole matrix elements for an atom with N electrons and normalization corrections.[19] The many-body dipole matrix elements are given by

$$Z_L=\left\langle\psi_f\left|\sum_{i=1}^{N}z_i\right|\psi_0\right\rangle \tag{2}$$

in the length form and

$$Z_V=\frac{1}{\omega}\left\langle\psi_f\left|\sum_{i=1}^{N}\frac{d}{dz_i}\right|\psi_0\right\rangle \tag{3}$$

in the velocity form. Here ψ_0 and ψ_f represent exact many-particle ground and final states with energy eigenvalues E_0 and E_f. In lowest order ψ_0 is given by the unperturbed state Φ_0 which satisfies

$$H_0\Phi_0=E_0^{(0)}\Phi_0\ , \tag{4}$$

where H_0 is the zeroth-order Hamiltonian

$$H_0=\sum_{i=1}^{N}\left[-\frac{\nabla_i^2}{2}-\frac{Z}{r_i}+V(r_i)\right]\ , \tag{5}$$

and the term $V(r_i)$ accounts for the average interaction of the ith electron with the remaining $N-1$ electrons. We usually choose $V(r_i)$ to be a Hartree-Fock potential. The residual interaction between electron pairs is given by

$$H_c=\sum_{i<j=1}^{N}v_{ij}-\sum_{i=1}^{N}V(r_i) \tag{6}$$

and is referred to as the electron-correlation perturbation in this paper. In Eq. (6) v_{ij} represents the Coulomb interaction between pairs of electrons.

The matrix elements Z_L and Z_V may be calculated by the methods of many-body perturbation theory,[19–21] evaluating the series of all open diagrams which contain one dipole interaction and any number of interactions with the electron-correlation perturbation of Eq. (6).[22]

The lowest-order diagrams in the dipole expansion for a transition $p\rightarrow k$ are shown in Figs. 1(a), 1(b), and 1(c). In these diagrams time increases from bottom to top. Hole states are represented by downward-pointing arrows and particle states by upward-pointing arrows. Dashed lines terminated by a dot are dipole interactions with the operator z (or d/dz in the velocity case) and other dashed lines are interactions with the correlation perturbation. Exchange diagrams, though not shown, are also included. The lowest-order term in the dipole expansion shown in Fig. 1(a) is $\langle k|z|p\rangle$ in the length formalism and $(1/\omega)\langle k|(d/dz)|p\rangle$ in the velocity formalism, where k and p are one-electron states calculated in the potential $V(r)$. Diagram 1(b) is first order in the correlation interaction and accounts for ground-state correlations (GSC); these occur prior to interactions with the radiation field. Closed loops in these diagrams imply sums over the (virtual) excited electron states. First-order final-state correlations (FSC) are represented by the diagram of Fig. 1(c). When the LS-coupled Hartree-Fock (HF) potential is used to calculate the excited orbitals, diagram 1(c) vanishes when p and q refer to the same subshell and k and k' have the same orbital angular momentum.[23] Second-order diagrams that are included in the RPAE formalism and iterated to all orders are shown in Figs. 1(d) and 1(e).

B. Relaxation effects

It has been shown previously that allowing for relaxation of the core electrons considerably alters the calculated cross section for photoionization of $4d$ electrons in barium.[8,9,11] Near threshold, the slow photoelectrons experience a change of potential as the core orbitals relax to become ionic orbitals. At sufficiently small photoelectron energies, it is reasonable to assume that relaxation is complete and to simulate the relaxation process near the photoionization threshold by calculating final-state orbitals in the potential of a relaxed ionic core. Such calculations have previously been carried out in low-order MBPT (Ref. 11) and in the RPAER method.[9] However, at higher energies, frozen core calculations are more realistic because the photoelectron can leave the atom before the remaining electrons have time to relax. In calculations with relaxed orbitals, overlap integrals $\prod_i\langle\phi_i'|\phi_i\rangle^{q_i}$

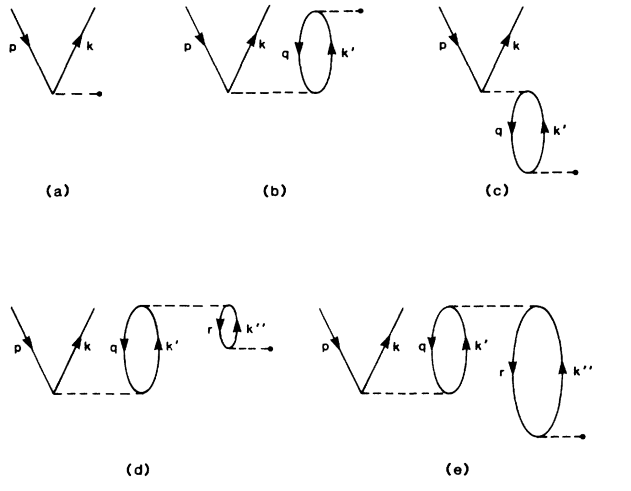

FIG. 1. Low-order Brueckner-Goldstone diagrams contributing to the dipole matrix element for photoionization. Time proceeds from bottom to top in these diagrams. Lines with arrows pointing downward represent hole states and lines with arrows pointing upward represent particle states. (a) Lowest-order dipole. (b) Ground-state correlation (GSC) diagram. (c) Final-state correlation (FSC) diagram. (d) and (e) RPAE diagrams. Dashed line ending with an isolated solid dot indicates matrix element of z. Other dashed lines represent the electron-correlation interaction.

between orbitals of the ground state ϕ_i and the corresponding orbitals of the final state ϕ_i' will appear in the many-body dipole matrix element for each subshell i of the ion with occupation number q_i. Permutations of the orbitals in overlap integrals are also included. The inclusion of overlap integrals in the evaluation of many-particle matrix elements is discussed by Löwdin.[24]

Relaxation effects may also be included by calculating the appropriate MBPT diagrams. Examples of such diagrams are shown in Figs. 2(a) and 2(b). The orbital r in Fig. 2(a) is perturbed due to the presence of the hole q and then interacts with the outgoing photoelectron. In Fig. 2(b), the time order of the interactions is reversed from Fig. 2(a). It should be noted that these diagrams do not include the effects of the overlap integrals.

The remaining diagrams in Figs. 2(c), 2(d), and 2(e) correspond to corrections to the energies of the hole states, a change in the effective potential of the outgoing electrons, and initial-state correlations, respectively. The diagram of Fig. 2(c) is a self-energy correction term which, when summed as part of a geometric series to infinite order, shifts the threshold for photoionization from the Hartree-Fock single-particle hole energy toward the experimental energy. Diagrams like Fig. 2(d) are called polarization diagrams. Here, the outgoing photoelectron excites the core and interacts with the excitation. Polarization of the initial state is represented by Fig. 2(e). The inclusion of diagrams typified by Fig. 2(d) and 2(e) is equivalent to the use of Brueckner orbitals in the final-state and ground-state wave functions.[25] Polarization diagrams account for the effects of doubly excited channels on the main-line channel. In Fig. 2(d) the single excitation channel ($p-k''$) interacts with the doubly excited channel ($pq\rightarrow k'k'''$), which in turn couples with the single excitation channel ($p\rightarrow k$). The interaction is with satellite states whenever either k' or k''' is a bound excited state and with double-photoionization channels when k' and k''' are both continuum states. It is possible for absorption flux to be redistributed from the main-line channel to doubly excited channels in this way or *vice versa*. When ω is sufficiently large, the two imaginary contributions that result from the vanishing energy denominators in the polarization diagrams [Fig. 2(d)] result in an overall minus sign for the polarization diagrams relative to the lowest-order dipole [Fig. 1(a)] and thus lead to an overall reduction in the photoionization cross section. The inclusion of overlap integrals in relaxed orbital method calculations is an approximate method which estimates some of the effects of the polarization diagrams and also leads to a reduced cross section.[17]

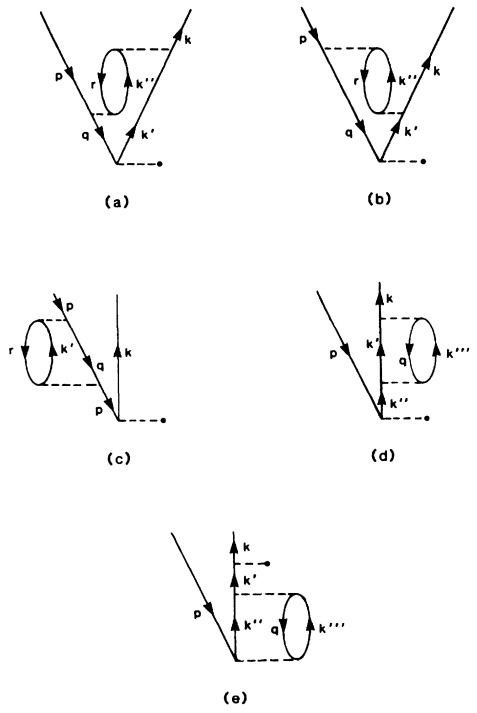

FIG. 2. (a)–(c): Diagrams contributing to core relaxation. Diagram (c) accounts for correlations in the hole energy. The effects of (c) may be included by using experimental threshold energies. (d) Final-state polarization diagram. (e) Ground-state polarization diagram.

C. Angular distribution

In the *LS*-coupling approximation, the angular asymmetry parameter can be expressed (for closed shells) as[26–28]

$$\beta=\frac{l(l-1)|R_{l-1}|^2+(l+1)(l+2)|R_{l+1}|^2-6l(l+1)\mathrm{Re}(\chi)}{(2l+1)[l|R_{l-1}|^2+(l+1)|R_{l+1}|^2]}\ , \tag{7}$$

where

$$\chi=R_{l-1}^{*}R_{l+1}e^{i(\delta_{l+1}-\delta_{l-1})}\ . \tag{8}$$

In Eqs. (7) and (8), $R_{l\pm1}$ represents the radial part of the dipole matrix elements which are complex due to the final-state correlations. The phase shifts $\delta_{l\pm1}$ in Eq. (8) represent the sum of the Coulomb and non-Coulomb parts.[26] The total phase shifts were determined from our single-particle continuum orbitals according to the Jeffries or WKB method[29] and contributions to the phase shifts are contained in the imaginary parts of $R_{l\pm1}$.

III. CALCULATION OF CROSS SECTIONS

Relaxation effects were included by explicit calculation of the relaxation diagrams of Figs. 2(a) and 2(b) and also by the approximate method of calculating final-state orbitals in the presence of the relaxed ionic core. In both cases the ground-state radial wave functions were generated with the Hartree-Fock code of Froese-Fischer.[30]

In the full MBPT calculation in which relaxation effects are calculated diagrammatically, continuum and bound *ks*, *kd*, *kp*, and *kf* orbitals were calculated in the

frozen-core Hartree-Fock V^{N-1} potentials derived from the couplings $5p^5ks(^1P)$, $5p^5kd(^1P)$, $4d^9kp(^1P)$, $5skp(^1P)$, $6skp(^1P)$, and $4d^9kf(^1P)$. For each angular momentum, 10 bound and 42 continuum orbitals were calculated with appropriate projection operators when necessary to ensure the orthogonality of the excited states to ground states of the same angular momentum.[31,32] The effect of the remainder of the bound excited states was taken into account by the n^{-3} rule[19] for diagrams contributing to correlations in the ground state. For diagrams contributing to correlations in the final state, higher bound states were included by explicit calculation and a back extrapolation of the continuum into the bound region.

The first-order GSC diagram of Fig. 1(b) was calculated for each photoionization channel $p \rightarrow k$ with the closed-loop channels $4d \rightarrow k'f,k'p$; $5p \rightarrow k'd,k's$; $5s \rightarrow k'p$; and $6s \rightarrow k'p$. First- and higher-order FSC, RPAE, and relaxation diagrams were included by using our coupled integral equations method.[33] This method is equivalent to the K-matrix method discussed, for example, by Starace.[26] In the coupled integral equations we included the intra- and interchannel interactions represented by diagram segments shown in Fig. 3. The labelings of the hole and particle lines in these diagram segments correspond to the dipole excitation channels of the $4d$, $5s$, $5p$, and $6s$ electrons. Figures 3(d) and 3(e) represent relaxation and Fig. 3(f) represents polarization of the $4d$, $5s$, $5p$, and $6s$ shells of the ionic core, and they were included in the $4d \rightarrow kf$ channels. In this manner the lowest-order relaxation and polarization diagrams of Figs. 2(a), 2(b), and 2(d) were included exactly and all higher-order diagrams repeating the segments of Figs. 3(d), 3(e), and 3(f) were included in an approximation which is expected to be very good. The diagrams of Figs. 2(a) and 2(b) with $p = 4d$ and $q = 5p$ were also included but were found to be small.

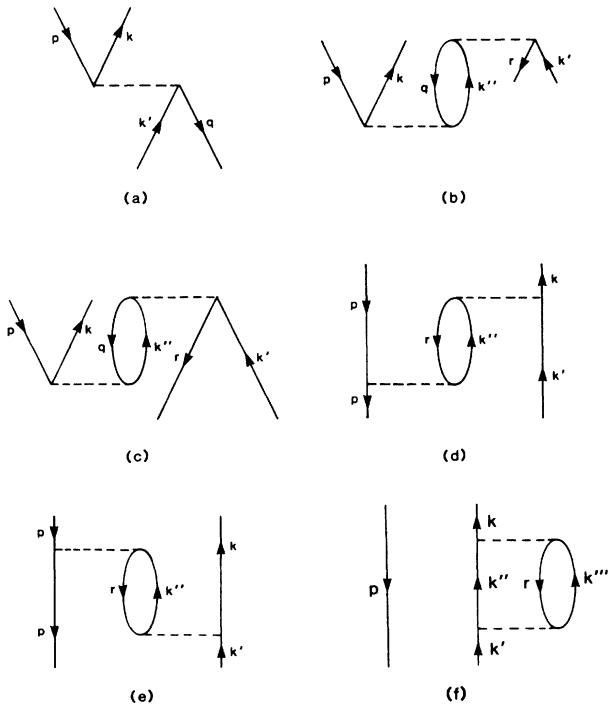

FIG. 3. Diagram segments contributing to inter- and intrachannel couplings included in the coupled equations method.

The diagram segments of Figs. 3(d), 3(e), and 3(f) were evaluated with excited states k'' and k''' calculated in a V^{N-1} potential with one electron missing from the shell represented by orbital r. The hole energy used was the Hartree-Fock eigenvalue from a self-consistent field calculation of the neutral atom.

We also investigated relaxation effects by calculating bound and continuum excited-state orbitals for the $4d \rightarrow kf$ channel in the potential of the relaxed $4d^9(^2D)$ core. We did not recalculate a relaxed set of kp excited orbitals since the contribution of the $4d^9kp$ channel to the $4d$ cross section is small (~ 1 Mb). We proceeded to higher order in MBPT evaluating GSC, FSC, and RPAE diagrams using excited orbitals calculated in the field of the relaxed ion. The coupled equations result was multiplied by the overlap integrals discussed in the preceding section. The overlap factor caused a 22% reduction in the barium $4d \rightarrow kf$ channel cross section and a 16% reduction in the $5p \rightarrow kd$ channel cross section, independent of energy.

The threshold energy used in the calculations was the 108.9-eV Hartree-Fock single-particle energy of the $4d$ electrons in barium. However, the calculations have been plotted starting at the experimental[34] threshold value of 99.3 eV, averaging over the $J = \frac{5}{2}$ and $J = \frac{3}{2}$ threshold energies according to statistical weights. This corresponds to plotting results as a function of photoelectron energy, which is frequently done.[26,28] Use of the experimental energy in the calculations corresponds to inclusion of the diagram of Fig. 2(c). Calculations performed using experimental threshold values yielded poorer length and velocity agreement but are similar to the shifted results when the geometric means of length and velocity cross sections are taken. Hansen[35] has shown that the geometric mean of length and velocity is less sensitive to correlations than either length or velocity and is therefore an appropriate choice when comparing theoretical results with experiment.

IV. RESULTS

A. Partial cross section of the $4d^{10}$ subshell

In this section we present our MBPT results obtained using the various techniques discussed above. These results are compared with the recent total absorption and photoemission measurements by Becker *et al.*[14] for the $4d$ partial cross section. Our results represent the photoemission $4d$ cross section and not the total absorption. The curve of total absorption is given so that the reader can judge the sum of contributions from satellite cross sections and double, triple, etc., photoionization.

In Fig. 4 we show the geometric mean of the $4d$ cross section in the frozen-core Hartree-Fock approximation (HF) and the Hartree-Fock approximation using relaxed

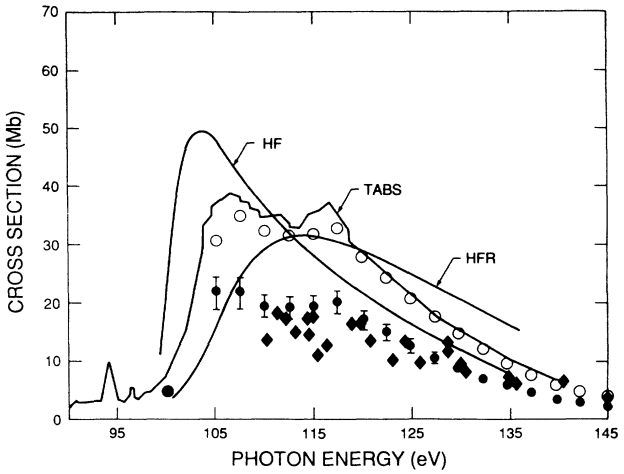

FIG. 4. Partial cross section for the $4d^{10}$ subshell of barium. HF is the geometric mean of lowest-order frozen-core Hartree-Fock length and velocity calculations from Ref. 11. HFR is the geometric mean of relaxed Hartree-Fock length and velocity cross sections, (Ref. 11). TABS is the total absorption measurement, (Ref. 7); ⧳ is the $4d^{10}$ photoemission measurement, (Ref. 14) and ○ is the sum of the $4d^{10}$ and satellites by Becker *et al.* (Ref. 15). ♦ is the partial $4d^{10}$ cross section measured by Bizau *et al.*[16] Our calculations should be compared with the photoemission experimental results and not with the total cross-section results or with the sum of $4d^{10}$ and satellites.

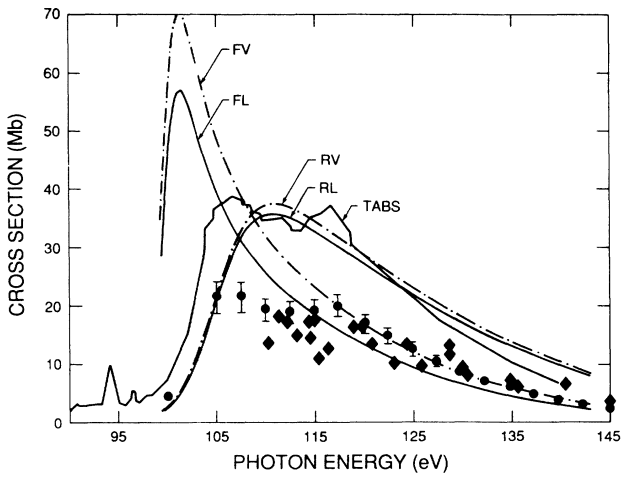

FIG. 5. Photoionization cross sections of atomic barium as a function of photon energy. TABS is the total absorption cross section (Ref. 7). ⧳ is the $4d$ partial cross-section measurement of Becker *et al.* (Ref. 14), and ♦ is the measurement of Bizau *et al.* (Ref. 16). Curves labeled FL and FV are MBPT calculations of the $4d$ partial cross section using orbitals calculated in the frozen-core potential (no relaxation effects are included in the FL and FV calculations). Curves labeled RL and RV are length and velocity MBPT calculations using relaxed orbitals but not including overlap integrals.

orbitals but not including overlap integrals (HFR) as obtained previously by Kelly *et al.*[11] The length and velocity results differ considerably in these low-order calculations. Also plotted are the total absorption (TABS) measurement of Richter *et al.*[7] and the $4d$ photoemission measurements (⧳) of Becker *et al.*[14] and (♦) of Bizau *et al.*[16] A measurement by Becker *et al.*[15] of the $4d$ main-line plus satellite contributions is also plotted (○). The HFR result is in fairly good agreement with the total absorption measurement but exceeds the photoemission measurement, particularly at higher energies. The sum of $4d$ main-line and satellite absorption shown in Fig. 4 is a large fraction of the total absorption. The contributions from $5s$, $5p$, and $6s$ photoemission total only a few Mb in this region.

In Fig. 5 we compare our present MBPT $4d$ length and velocity cross sections without relaxation (FL and FV) with the partial $4d$ cross section of Becker *et al.*[14] (⧳), and Bizau *et al.*[16] (♦), and the total absorption cross section[7] (TABS). The FL and FV notation refers to frozen-core length and velocity results, respectively. The FL and FV results include both initial-and final-state correlations among the six channels discussed in Sec. III. The FL and FV curves also include diagrams of the RPAE type [Figs. 1(d) and 1(e)], and it is these diagrams that have caused the drastic change in the cross section from the low-order result.[10] Our frozen-core results rise very rapidly from the threshold, peak at an energy which is low compared with the experimental peak, and then rapidly decrease to values compared with the $4d$ photoemission measurement at high energies. Correlations have caused the velocity calculation to exceed the length calculation in magnitude, a reversal of the order in lowest-order calculations. The curves labeled RL and RV are similar calculations to those of the curves FL and FV but use relaxed orbitals and do not include overlap integral factors. Our calculated results are intended to correspond to photoemission results and at this point do not agree well with the photoemission experimental results.[14,16] However, it will be seen later that inclusion of overlap integrals in the calculations with relaxed orbitals are in better agreement with experiment. Again, we include the total absorption results[7] (TABS) so that effects of satellite contributions and multiple ionizations may be seen.

Weak excitations appear in many of the total absorption spectra[2-6] between 100 and 105 eV, although they are not seen in the present plots of TABS, which have been attributed to the simultaneous excitations of $4d$ and $5p$ electrons.[1] Since the single-particle energy of a $6s$ electron is about 5 eV, it is also possible that these are double-electron resonances involving the excitations of $4d$ and $6s$ electrons simultaneously. Stronger features between 110 and 120 eV are probably due to the simultaneous excitation of $(4d,5p)$ and $(4d,5s)$ electron pairs. Wendin[36] has suggested that resonances due to $4d^{10}5s^25p^6 \rightarrow 4d^95s^25p^55d^2$ excitations may be responsible for structure in this region.

Calculations including relaxation effects by diagrams (but not including polarization diagrams) are compared with experiments in Fig. 6. The curves labeled RDL and RDV are length and velocity calculations, respectively, in which the relaxation effects were included by calculating

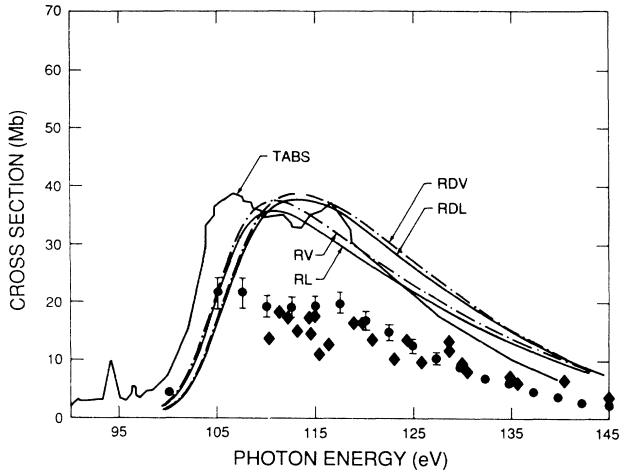

FIG. 6. Photoionization cross sections of barium as a function of photon energy. TABS is the experimental total absorption cross section, (Ref. 7), ⧳ is the measured $4d$ partial cross section of Ref. 14, and ♦ is from Ref. 16. RDL and RDV are MBPT length and velocity calculations which include relaxation diagrams. RL and RV include relaxation effects using relaxed orbitals but not including overlap integrals.

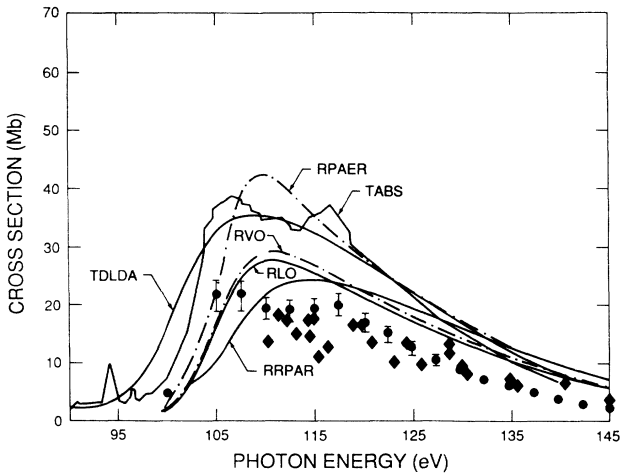

FIG. 7. Barium $4d$ photoionization cross sections. ⧳, experiment from Ref. 14, and ♦, experiment from Ref. 16. RLO and RVO are length and velocity MBPT calculations using relaxed orbitals and including overlap integrals. RPAER is the random-phase approximation with exchange calculation with relaxation effects by Amusia *et al.* (Ref. 9). TDLDA is the time-dependent local-density-approximation calculation by Zangwill and Soven (Ref. 12). RRPAR is a relativistic random-phase-approximation calculation with relaxation and overlap by Radojević *et al.* (Ref. 17).

the diagrams of Figs. 2(a) and 2(b) with $p=q=4d$ and $r=4d,5s,5p,6s$ in addition to other correlation effects shown in Fig. 1. Higher-order relaxation diagrams were approximately included in the coupled equations calculations as already discussed. The interactions among channels originating from the $4d,5s,5p$, and $6s$ subshells were included to all orders by the coupled equations method discussed in Sec. II. The curves labeled RL and RV in Fig. 6 represent correlated length and velocity MBPT cross sections using relaxed orbitals but without inclusion of overlap factors. We expect the RDL, RDV, and RL and RV calculations to be in reasonable agreement for energies near threshold. The discrepancy between the calculations and the photoemission $4d$ partial cross sections persists beyond the peak when relaxation is included by either method. Length and velocity results have been brought into closer agreement by inclusion of relaxation effects.

In Fig. 7 we present the time-dependent local-density-approximation calculation[12], the random-phase approximation with exchange calculation using relaxed orbitals[9], the relativistic random-phase approximation calculation using relaxed orbitals[17] (RRPAR), our relaxed orbital method calculation including overlaps (RLO, RVO), the experimental $4d$ partial cross section,[14,16] and the total absorption measurements of Richter *et al.*[7] The total absorption has been scaled to agree with the TDLDA calculation[12] at 110 eV. It has been customary[9,12] to compare the RPAER and TDLDA calculations with total absorption experiments. The RRPAR, RLO, and RVO calculations should be compared with the photoemission results. Incorporation of overlap integrals in the MBPT calculation has lowered the overall cross section by 22% at all energies. Most of this overlap factor is due to the readjustment of the two $6s$ orbitals. The overlap $\langle 6s'|6s\rangle$ is 0.952, where $|6s'\rangle$ is the $6s$ orbital for the ion $4d^{-1}$ and $|6s'\rangle$ is the $6s$ orbital of neutral ground-state barium. This method simplifies the inclusion of higher-order relaxation effects, but still does not correctly describe the photoemission cross section at energies just above the peak. The RRPAR result[17] agrees fairly well with the MBPT calculations; differences between these two results are due partly to relativistic effects and the fact that the RRPAR formalism iterates the diagrams of Fig. 1 to all orders. The MBPT calculations treat the ground-state correlation diagram of Fig. 1(b) to first order, the final-state correlation diagram of Fig. 1(c) to all orders, and most of the RPA diagrams of Figs. 1(d) and 1(e) to all orders by insertion of RPA diagram segments [Figs. 3(b) and 3(c)] into the coupled equations.[33] Radojević *et al.*[17] compare two unrelaxed calculations of the $4d$ cross section obtained using the RPAE and the RRPA and demonstrate that relativistic effects lower the peak value of the cross section. Including relativistic effects in the MBPT calculations should tend to reduce the $4d$ cross section in the vicinity of the peak.

Calculations which include both relaxation and polarization diagrams are plotted in Fig. 8 along with the photoemission results[14,16] and the correlated results which do not include any relaxation or polarization effects (FL and FV). The curves labeled RPL and RPV are length and velocity calculations, respectively, in which relaxation diagrams were included as before and polarization effects were included by calculating the diagram segments of Fig. 3(f) with $p=4d$ and $r=4d,5p,5s,6s$ and inserting the segments into the coupled equations. This adds the dia-

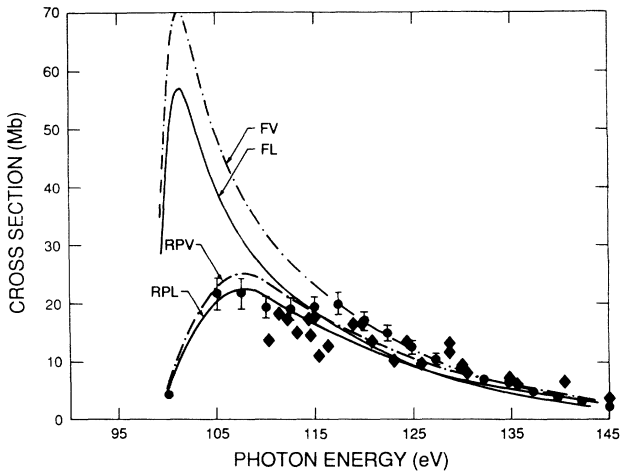

FIG. 8. Barium partial $4d$ photoionization cross sections. ⏀, experiment from Ref. 14, and ♦, from Ref. 16. FL and FV are length and velocity MBPT calculations without relaxation. RPL and RPV are MBPT length and velocity calculations which include both relaxation and polarization diagrams.

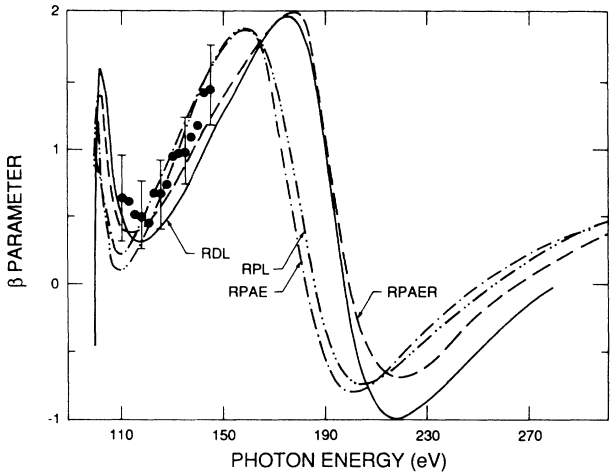

FIG. 9. The angular distribution asymmetry parameter β as a function of photon energy for photoelectrons from the $4d^{10}$ subshell. Correlated length (——, RDL) calculation in MBPT including relaxation diagrams; length calculation in MBPT including relaxation and polarization diagrams (– – ··, RPL), — — —; RPAER calculation, (Ref. 9); —·—·—·, RPAE calculation (without relaxation) (Ref. 9); ◇, experimental points by Becker *et al.* (Ref. 14).

gram of Fig. 2(d) as well as higher-order diagrams which repeat the interactions along the particle line. The diagram of Fig. 2(e) is less important because it has two energy denominators which contain the hole energy of the $4d$ electron and no ω which cancels the $4d$ hole energy in the diagrams which have polarization and relaxation in the final state. This makes it smaller than the final-state polarization diagrams by an order of magnitude. We have not included the diagram of Fig. 2(e) in the present calculation. For photoionization of outer electrons, however, the diagram of Fig. 2(e) may become very significant. In the vicinity of the peak, we obtain reasonable agreement with the photoemission experiment, but at higher energies the calculations are slightly below the experimental values. Above 130 eV the polarization diagrams seem to approximately cancel the relaxation diagrams, i.e., the RPL and RPV results approach the unrelaxed results FL and FV at high energy. It is difficult to ascribe great accuracy to these calculations because the diagrams which are second order in the correlation (RPAE, relaxation, and polarization) exhibit large cancellation. The barium $4d$ cross section seems to be very sensitive to higher-order effects. Similar calculations in xenon (which does not have the pair of $6s$ electrons in the ground state) appear to be less sensitive to these effects.[37]

The angular distribution asymmetry parameter for the $4d$ subshell is plotted in Fig. 9. The curves labeled RPAE and RPAER in this figure represent the random-phase approximation calculations of Amusia *et al.*,[9] with relaxed orbitals for the RPAER calculation. In our calculations we used correlated dipole matrix elements obtained from the diagrammatic method for relaxation. These results are labeled RDL; only the length result is shown because of the very close agreement between length and velocity results. We also present results obtained from the diagrammatic method for relaxation and polarization (RPL). A partial cancellation between the relaxation and polarization diagrams may be seen in the β parameter as in the $4d$ partial cross section. The experimental data are by Becker *et al.*[14] The experimental results seem to agree best with the unrelaxed RPAE result and the RPL result.

B. Partial cross sections for $6s^2$, $5s^2$, and $5p^6$

We now present calculations of the photoionization cross sections for the $6s^2$, $5s^2$, and $5p^6$ subshells near their respective thresholds as well as in the region of enhancement near the $4d$ threshold. Experimental data is now available for these cross sections below the $4d$ threshold[16] and provides important tests of many-body theories.

Figure 10 is a plot of our $6s \rightarrow kp$ cross section. The dashed (dotted) line is our MBPT length (velocity) result without the inclusion of relaxation or polarization effects. The cross-section measurement near threshold by Hudson *et al.*[38] is represented by triangles. In this region there are many double-electron resonances which we have not attempted to calculate but have been calculated by Bartschat *et al.*[39] using R-matrix theory. The data from Hudson *et al.*[38] were selected between resonances so that the large-scale behavior may be seen. More recent measurements[40] suggest that the Hudson *et al.*[38] cross section may be too small by a factor of 5. The present MBPT calculation does not unambiguously favor one normalization over the other because of the steepness of the cross section below the Cooper minimum and the existence of a double-electron resonance just above the $6s$ threshold. The large autoionizing resonance at 19.8 eV is the $5p^5 5d(^1P)$ resonance originally discussed by Wendin.[41] Since spin-orbit effects and double-electron resonances were not included in the present calculation,

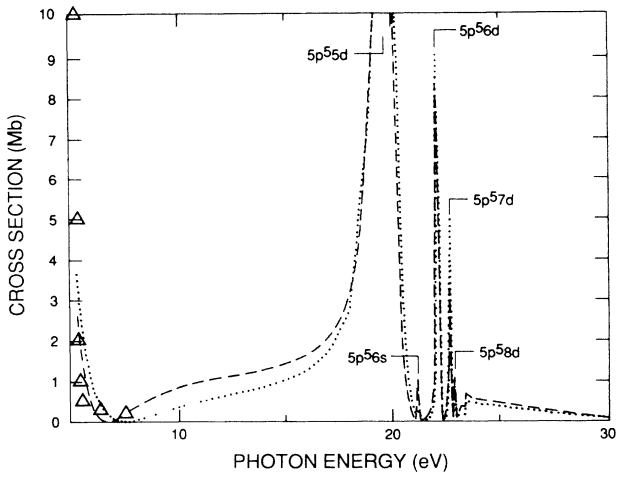

FIG. 10. Photoionization cross section of the $6s^2$ subshell of barium. — — —, MBPT length calculation; · · · ·, MBPT velocity calculation (spin-orbit splitting of resonances not included); △, measured photoionization cross section (Ref. 38).

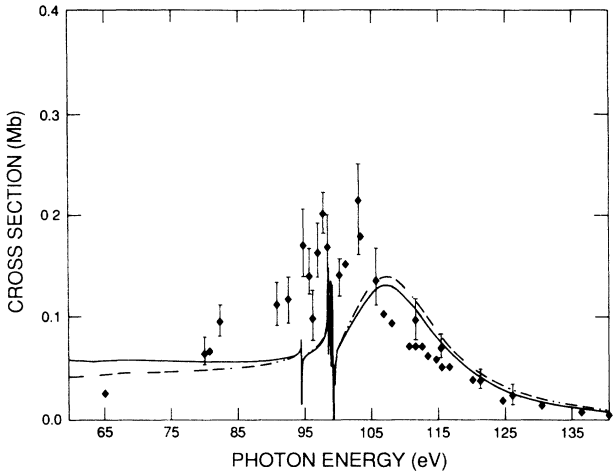

FIG. 12. Barium 6s photoionization cross section in vicinity of 4d threshold. ——, MBPT length, and – –··, MBPT velocity calculations; ◇, photoemission measurement of Bizau *et al.* (Ref. 16).

agreement with experiment is not expected to be good.

The $6s \rightarrow kp$ cross section is plotted in Fig. 11 from the 5p threshold (24.71 eV) to 50 eV. The data for the 6s cross section are photoelectron spectroscopy measurements by Bizau *et al.*[16] normalized by matching experimental and TDLDA (Ref. 13) 5p cross sections at the peak. Interchannel coupling with the 5p and 4d channels causes the 6s cross section to drop abruptly from a maximum value at the 5p edge to a minimum at 34 eV. Relaxation effects were not included in the 6s or 5p channels in the MBPT calculation. It is interesting to note that the theoretical result is too small relative to experiment near the 5p threshold whereas the calculated 5p cross sections are larger than experiment near threshold as we shall see.

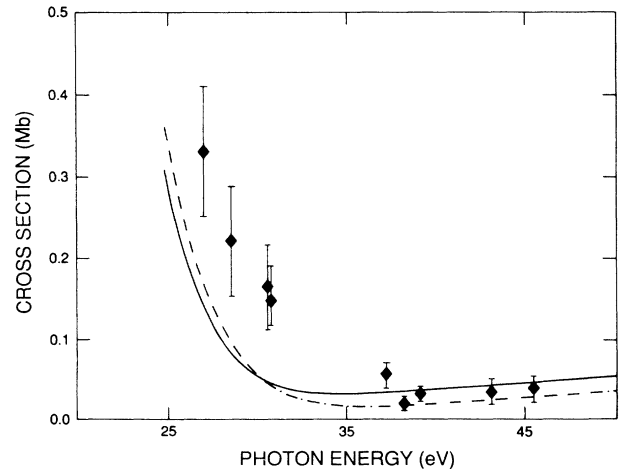

FIG. 11. Photoionization cross section for 6s electrons in barium for photon energies just above the 5p threshold. ——, MBPT length, and —·—·—·, MBPT velocity; ♦, photoemission measurements of Bizau *et al.* (Ref. 16).

The $6s \rightarrow kp$ photoionization cross section in the vicinity of the large 4d absorption is shown in Fig. 12 along with recent measurements by Bizau *et al.*[16] The curves labeled MBPTL and MBPTV are length and velocity calculations which include correlations; relaxation diagrams were included in the $4d \rightarrow kf$ channel. Spin-orbit splittings have not been included in the calculation of resonances below the 4d threshold. The MBPT results are in reasonable agreement with experiment above 110 eV. In

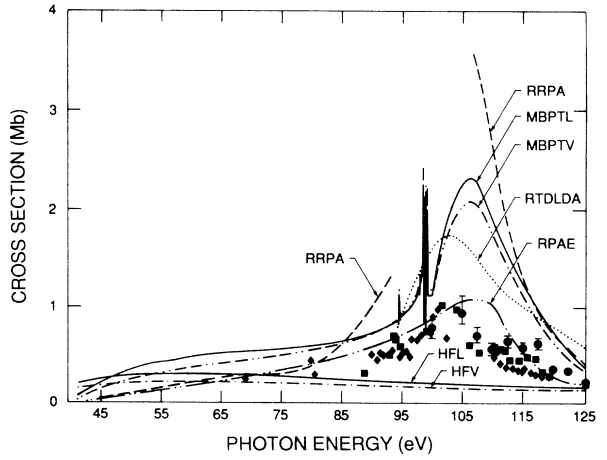

FIG. 13. Photoionization cross section of $5s^2$ subshell of barium as a function of photon energy. HFL and HFV are Hartree-Fock length and velocity results, respectively. MBPTL and MBPTV are correlated length and velocity results. Spin-orbit splitting of resonances is not included. RPAE result (–··), from Ref. 44. RRPA is the relativistic random-phase-approximation calculation obtained using the code of Johnson *et al.* (Ref. 43). TDLDA is the time-dependent local-density approximation (Ref. 13). ■, Richter *et al.* (Ref. 7), photoemission measurement; ●, experiment by Becker *et al.* (Ref. 14); ♦, experiment by Bizau *et al.* (Ref. 16).

the region between 90 and 105 eV the calculations appear too small. Some of the discrepancy is due to the presence of autoionizing resonances in the 6*s* cross section below the 4*d* threshold. Many of the measured data points are in the resonance region. A discrepancy remains, however, just above the 4*d* threshold. It may be that coupling the 6*s* channel with the 4*d* channel including relaxation diagrams does not represent the interaction between 6*s* and 4*d* satellite channels well.

The $5s \rightarrow kp$ cross section is plotted in Fig. 13. The HFL and HFV curves are Hartree-Fock length and velocity results. The MBPTL and MBPTV curves are length and velocity results obtained by coupling the $5s \rightarrow kp$ channel with the $4d \rightarrow kf$, $4d \rightarrow kp$, $5p \rightarrow kd$, $5p \rightarrow ks$, and $6s \rightarrow kp$ channels; relaxation diagrams were included in the $4d \rightarrow kf$ channel. Autoionizing resonances $4d^9np(^1P)$ and $4d^9nf(^1P)$ may be seen below the 4*d* photoionization threshold. We have not included the 4*d* spin-orbit splitting. Also plotted are the RPAE results of Amusia,[42] a time-dependent local-density-approximation (TDLDA) calculation,[13] and a relativistic random-phase calculation which we have obtained using the code developed by Johnson *et al.*[43] The experimental data of Becker *et al.*,[14] Richter *et al.*,[7] and Bizau *et al.*[16] are indicated by closed circles (⏀), squares (■), and diamonds (♦), respectively. The Hartree-Fock eigenvalue energy (41.16 eV) was used for the 5*s* threshold in the MBPT calculation. It is interesting to note that correlations have lowered the 5*s* cross section near threshold. This is in contrast to the xenon 5*s* cross section where correlations with 5*p* and 4*d* shells significantly raised the value of the cross section near threshold.[44]

The calculations vary widely in the 4*d* shape resonance region. The RRPA calculation attains the highest peak value because relaxation effects were not included on the 4*d* channel which is driving the 5*p* and other weak channels. It is not at all clear why the early RPAE calculation of Amusia[42] is not at least as large as the RRPA calculation since relaxation was not included in the RPAE calculation either. That the TDLDA (Ref. 13) and MBPT calculations are too large is not surprising because of the neglect of interactions mixing the pure single 5*s* va-

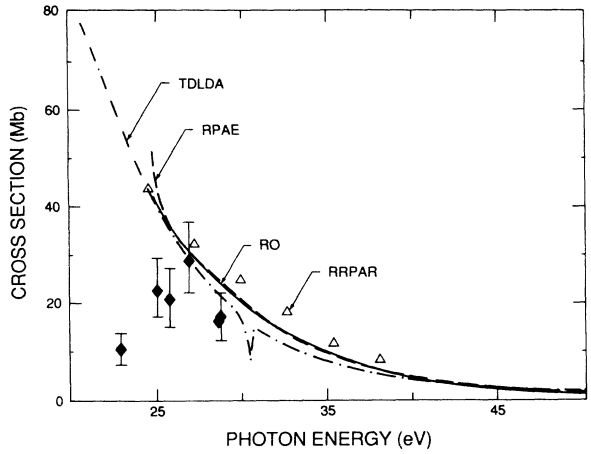

FIG. 15. Photoionization cross section calculations of the $5p^6$ subshell of barium. RO is the geometric mean of length and velocity MBPT calculations using orbitals calculated in a relaxed ionic potential and including overlap integrals. △, relativistic random-phase-approximation calculations including relaxation effects and overlap integrals (RRPAR) (Ref. 17); – – –, the random-phase-approximation (RPAE) calculation of Amusia *et al.* (Ref. 28); –·–·–·, the time-dependent local-density approximation (TDLDA) calculation of Nuroh *et al.* (Ref. 47); ♦, experimental results by Bizau *et al.* (Ref. 16).

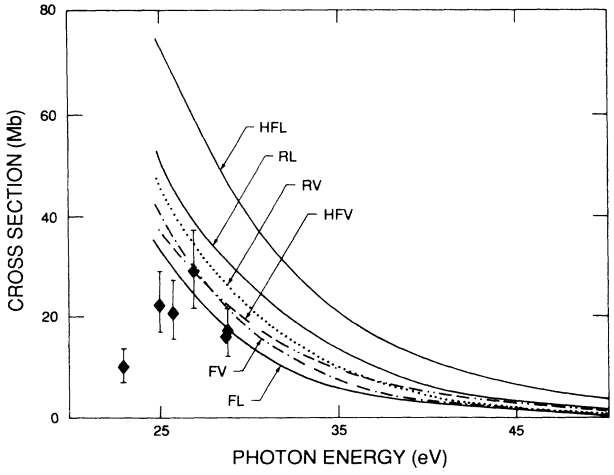

FIG. 14. Calculations of the $5p^6$ photoionization cross section near threshold. HFL and HFV are Hartree-Fock length and velocity calculations. FL and FV are correlated, frozen-core, length and velocity calculations. RL and RV are length and velocity results including correlations and using the relaxed orbital method without including overlap integrals. ♦, experimental results by Bizau *et al.* (Ref. 16).

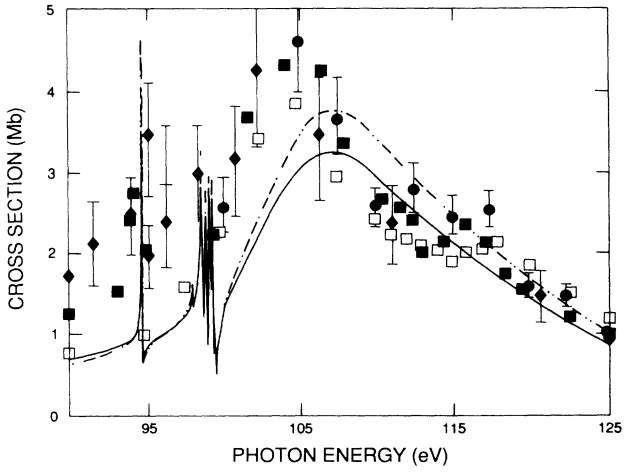

FIG. 16. Photoionization cross section of $5p^6$ subshell of barium in the vicinity of the 4*d* threshold. ——, MBPT length calculation; – –··, MBPT velocity calculation; □, solid state measurements (Ref. 5). Photoemission measurements are ■, Richter *et al.* (Ref. 7); ⏀, Becker *et al.* (Ref. 14); and ♦, Bizau *et al.* (Ref. 16).

cancy with more complex multiple excitations.[45] The effect of such mixing was discussed by Amusia[46] in terms of the spectroscopic factor which reduces the single-excitation cross section significantly. In xenon, the spectroscopic factor reduces the 5*s* cross section by 66% as determined by photoelectron spectroscopy experiments.[45] Such effects are expected to be stronger in the present case of barium 5*s* photoionization.

In Fig. 14 we have plotted calculations of the 5*p* cross section near threshold. The Hartree-Fock length and velocity results are plotted as HFL and HFV, respectively. The curves FL and FV are frozen-core length and velocity MBPT calculations which include correlations but no relaxation effects. The effect of correlations is to bring the length and velocity results into better agreement and also to lower the overall result. The curves labeled RL and RV are results obtained by the relaxed orbital method including correlations but not including overlap integrals. We have used the Hartree-Fock threshold energy of 24.71 eV (this is to be compared to the experimental threshold[34] of 23.41 eV). The data with error bars are from a very recent measurement obtained from the intensity of the Auger lines by Bizau *et al.*[16]

Additional calculations of the 5*p* cross section are shown in Fig. 15. The geometric mean of our relaxed orbital calculations of Fig. 11 multiplied by the overlap integral factor (in this case, 0.84) is given by the solid curve labeled RO. The RRPAR results, obtained using a modified version of the relativistic random-phase approximation (RRPA) code of Johnson *et al.*[43] are given by open triangles (△). The RPAE result of Amusia and Cherepkov[28] and the TDLDA result of Nuroh *et al.*[47] are also plotted. The sudden dip in the TDLDA calculation is attributed to the $5s6p(^1P)$ resonant state.[47] Our calculations did not sample enough frequencies below the 5*s* threshold to map out the autoionizing resonances in that spectral region. The measured cross section of Bizau *et al.*[16] is given by triangles and generally is smaller than all of the theoretical results. In a future study we hope to investigate the effects of relaxation and polarization diagrams on the 5*p* cross section near threshold to determine whether these effects can account for the discrepancies between theory and experiment.

The 5*p* cross section in the vicinity of the 4*d* threshold is shown in Fig. 16. The solid and dot-dashed curves are length and velocity results including relaxation diagrams for the 4*d* channel. The length and velocity discrepancy would be reduced if the Hartree-Fock single-particle 4*d* energy were used for the 4*d* channels rather than the experimental energy. We used the experimental 4*d* hole energy so that the $4d^9np(^1P)$ and $4d^9nf(^1P)$ resonances would be in the correct locations. Spin-orbit splitting has not been included. The experimental data points indicated by □ are due to Hecht and Lindau[5] (solid state). Data indicated by ■, ⧲, and ♦ are by Richter *et al.*,[7] Becker *et al.*,[14] and Bizau *et al.*,[16] respectively, and represent partitions of the total absorption for atomic barium.

The angular distribution asymmetry parameter β of the $5p^6$ shell is also of interest, especially with regard to the coupling between the 5*p* and 4*d* channels. MBPT length and velocity calculations which include the interchannel coupling are plotted in Fig. 17 along with Hartree-Fock (HFL and HFV). Correlations introduce a significant increase in β in the energy region of significant 4*d* photoionization. The correlated results are in favorable agreement with the experimental data of Becker *et al.*[14]

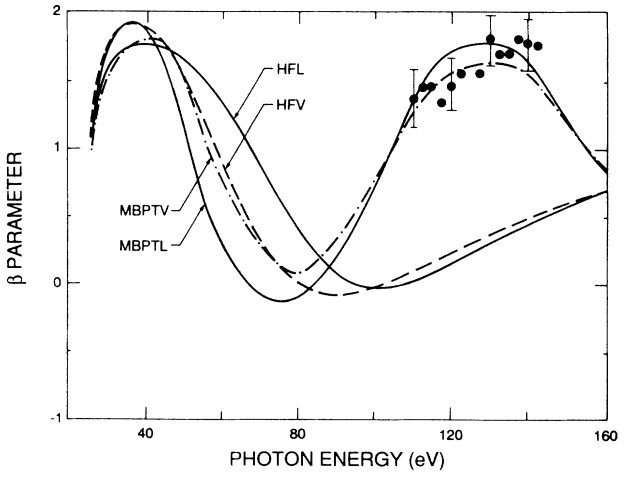

FIG. 17. Angular distribution asymmetry parameter β for the $5p^6$ subshell of barium as a function of photon energy. HFL and HFV are Hartree-Fock length and velocity calculations. MBPTL and MBPTV are many-body length and velocity calculations which include interchannel couplings with the 4*d* channels. ⧲, experimental data points by Becker *et al.* (Ref. 14).

V. DISCUSSION AND CONCLUSIONS

We have studied higher-order many-body effects on the photoionization cross sections of barium and have found that both relaxation and polarization effects must be included in the theory if agreement with recent 4*d* photoemission measurements[14,16] is to be obtained. Two different methods have been used to study these effects: (i) Higher-order diagrams in MBPT have been summed to account for relaxation and polarization and (ii) excited-state wave functions have been calculated in the potential of a relaxed ionic core to approximate relaxation, with the resulting overlap integrals approximating polarization. When relaxation is not included, the calculations are much too high in the energy range from threshold to the peak and also the peak value is too high. The agreement at higher energies is better. When relaxation effects are included, either diagrammatically or by using relaxed orbitals, the agreement between calculations and the total absorption measurements are quite good. However, relaxation alone gives results which are high compared with the 4*d* partial cross section, particularly beyond the peak in the cross section.

Becker *et al.*[15] have measured absorption due to satellite channels and find that this absorption accounts for most of the difference between the total absorption results and the 4*d* photoemission results. We have found that in order to calculate accurately the 4*d* photoionization cross section, it is necessary to include higher-order diagrams

which can account for the loss of flux from the $4d \rightarrow kf, kp$ channel to the satellite channels. The polarization diagrams of Fig. 2(d) represent the lowest-order diagrams which transfer flux from the main-line channels to the satellite channels. We have seen that including polarization diagrams in the calculation lowers the overall result, especially above the peak where inclusion of relaxation alone gives a result which is too high. The calculation of the $4d$ and $5p$ cross sections of barium is very sensitive to these higher-order relaxation and polarization diagrams and therefore must not be assigned great accuracy.

The present MBPT calculations are nonrelativistic; by comparing the MBPT results with the RRPA results of Radojević *et al.*,[17] it appears that relativistic effects are not negligible. Relativistic effects, such as spin-orbit splitting of the $4d_{5/2}$ and $4d_{3/2}$ thresholds, tend to reduce the cross-section peak as well as redistribute some of the oscillator strength to higher energies.

An approximate and simple way to make an estimate of the loss of flux to other channels is to use relaxed orbitals and include overlap integrals as discussed in this paper. We have found a 22% reduction of the barium $4d$ cross section due to overlap integrals. However, this reduction occurs at all energies and fails to account for the increased reduction needed beyond the peak. It is only when relaxation and polarization effects are included diagrammatically that agreement can be obtained at all energies. Overlap integrals cause a 16% reduction in the relaxed $5p$ cross section.

It would be of great interest to calculate the strength and effects of satellite channels by directly including them in a coupled equations calculation[33] as has been done for argon.[48] Absorption due to double-ionization channels could also be calculated through a given order in perturbation theory. Such calculations would show directly where the absorption flux is diverted.

ACKNOWLEDGMENTS

We wish to thank Dr. Daniel Frye, Dr. Cheng Pan, Dr. Wasantha Wijesundera, Dr. V. Radojević, and Dr. J. Cooper for their helpful ideas. We are also grateful to the National Science Foundation for financial support.

*Permanent address: Marmara University, Istanbul, Turkey.

[1] *Giant Resonances in Atoms, Molecules, and Solids,* Vol. 151 of *NATO Advanced Study Institute, Series B: Physics,* edited by J. P. Connerade, J. M. Esteva, and R. C. Karnatak (Plenum, New York, 1987).

[2] R. Rabe, K. Radler, and H. W. Wolff, in *VUV Radiation Physics,* edited by E. E. Koch, R. Haensel, and C. Kunz (Pergamon Vieweg, Braunschweig, 1974).

[3] J. P. Connerade and M. W. D. Mansfield, Proc. R. Soc. London, Ser. A **341**, 267 (1974).

[4] D. L. Ederer, T. B. Lucatorto, E. B. Saloman, R. P. Madden, and J. Sugar, J. Phys. B **8**, L21 (1975).

[5] M. H. Hecht and I. Lindau, Phys. Rev. Lett. **47**, 821 (1981).

[6] T. B. Lucatorto, T. J. McIlrath, J. Sugar, and S. M. Younger, Phys. Rev. Lett. **47**, 1124 (1981).

[7] M. Richter, M. Meyer, M. Pahler, T. Prescher, E. V. Raven, B. Sonntag, and H. E. Wetzel, Phys. Rev. A **39**, 5666 (1989).

[8] G. Wendin, Phys. Lett. **51A**, 291 (1975).

[9] M. Ya. Amusia, V. K. Ivanov, and L. V. Chernysheva, Phys. Lett. **59A**, 191 (1976).

[10] A. W. Fliflet, R. L. Chase, and H. P. Kelly, J. Phys. B **7**, L443 (1974).

[11] H. P. Kelly, S. L. Carter, and B. E. Norum, Phys. Rev. A **25**, 2052 (1982).

[12] A. Zangwill and P. Soven, Phys. Rev. Lett. **45**, 204 (1980).

[13] G. Wendin, in *New Trends in Atomic Physics,* 1982 Les Houches Lectures, edited by G. Grynberg and R. Stora (Elsevier, New York, 1984), p. 557.

[14] U. Becker, H. G. Kerkhoff, M. Kupsch, B. Langer, A. Sivasli, and R. Wehlitz (unpublished).

[15] U. Becker, in *Giant Resonances in Atoms, Molecules, and Solids,* Vol. 151 of *NATO Advanced Study Institute, Series B: Physics,* edited by J. P. Connerade, J. M. Esteva, and R. C. Karnatak (Plenum, New York, 1987), p. 473; U. Becker, R. Hölzel, H. G. Kerkhoff, B. Langer, D. Szostak, and R. Wehlitz, in *Abstracts of Contributed Papers, Fourteenth International Conference on the Physics of Electronic and Atomic* Collisions, Palo Alto 1985, edited by M. J. Coggiola, D. J. Huestis, and R. Saxon (ICPEAC, Palo Alto, 1985), p. 12.

[16] J. M. Bizau, D. Cabaynes, P. Gerard, and F. J. Wuilleumier, Phys. Rev. A **40**, 3002 (1989).

[17] V. Radojević, M. Kutzner, and H. P. Kelly, Phys. Rev. A **40**, 727 (1989).

[18] U. Fano and J. W. Cooper, Rev. Mod. Phys. **40**, 441 (1968).

[19] H. P. Kelly, Adv. Theor. Phys. **2**, 75 (1968).

[20] K. A. Brueckner, Phys. Rev. **97**, 1353 (1955).

[21] J. Goldstone, Proc. R. Soc. London, Ser. A **239**, 267 (1957).

[22] H. P. Kelly and A. Ron, Phys. Rev. A **5**, 168 (1972).

[23] M. Ya. Amusia, N. A. Cherepkov, and L. V. Chernysheva, Zh. Eksp. Teor. Fiz. **60**, 160 (1971) [Sov. Phys.—JETP **33**, 90 (1971)].

[24] P. Löwdin, Phys. Rev. **97**, 1474 (1955).

[25] I. Lindgren and J. Morrison, *Atomic Many-Body Theory* (Springer-Verlag, Berlin, 1982), p. 260.

[26] A. F. Starace, in *Corpuscles and Radiation in Matter I,* Vol. 31 of *Handbuch der Physik,* edited by W. Melhorn (Springer-Verlag, Berlin, 1982), p. 1.

[27] J. W. Cooper and R. N. Zare, in *Lectures in Theoretical Physics,* edited by S. Geltman, K. Mahanthoppa, and W. Brittin (Gordon and Breach, New York, 1969), Vol. XI-C.

[28] M. Ya. Amusia and N. A. Cherepkov, Case Stud. At. Phys. (Netherlands) **5**, (No. 2), 47 (1975).

[29] A. Burgess, Proc. Phys. Soc. London **81**, 442 (1963).

[30] C. Froese-Fischer, Comput. Phys. Commun. **14**, 145 (1978).

[31] S. Huzinaga and C. Arnau, Phys. Rev. A **1**, 1285 (1970).

[32] J. H. Silverstone and M. L. Yin, J. Chem. Phys. **49**, 2026 (1968).

[33] E. R. Brown, S. L. Carter, and H. P. Kelly, Phys. Rev. A **21**, 1237 (1980).

[34] H. Siegbahn and L. Karlsson, in *Corpuscles and Radiation in Matter I,* Vol. 31 of *Handbuch der Physik,* edited by W. Melhorn (Springer-Verlag, Berlin, 1982), p. 215.

[35] A. E. Hansen, Mol. Phys. **13**, 425 (1967).

[36] G. Wendin, in *VUV Radiation Physics,* edited by E. E. Koch, R. Haensel, and C. Kunz, Pergamon Vieweg, Braunschweig, 1974), p. 225.

[37] Z. Altun, M. Kutzner, and H. P. Kelly, Phys. Rev. A **37**, 4671 (1988).

[38]R. D. Hudson, V. L. Carter, and P. A. Young, Phys. Rev. A **2**, 643 (1970).
[39]K. Bartschat, M. R. H. Rudge, and P. Scott, J. Phys. B **19**, 2469 (1986).
[40]J. L. Carlsten and T. C. McIlrath, J. Phys. B **6**, L284 (1973); E. B. Saloman, J. W. Cooper, and G. Mehlman, Phys. Rev. A **32**, 1878 (1985).
[41]G. Wendin, Phys. Lett. **46A**, 119 (1973).
[42]M. Ya. Amusia, in Ref. 36, p. 205.
[43]W. R. Johnson and C. D. Lin, Phys. Rev. A **20**, 978 (1979); W. R. Johnson, C. D. Lin, K. T. Cheng, and C. M. Lee, Phys. Scr. **21**, 409 (1980).
[44]M. Ya. Amusia, Adv. At. Mol. Phys. **17**, 1 (1981).
[45]J. E. Hansen, Comments At. Mol. Phys. **12**, 3 (1982); **12**, 197 (1982).
[46]M. Ya. Amusia, Comments At. Mol. Phys. **16**, 143 (1985).
[47]K. Nuroh, E. Zaremba, and J. J. Stott, in *Giant Resonances in Atoms, Molecules, and Solids,* Vol. 151 of *NATO Advanced Study Institute, Series B: Physics,* edited by J. P. Connerade, J. M. Esteva, and R. C. Karnatak (Plenum, New York, 1987), p. 115.
[48]W. Wijesundera and H. P. Kelly, Phys. Rev. A **39**, 634 (1989).